

Article

Bimetal/Li₂Se Nanocomposite as Cathode Prelithiation Additive for Sustainable High-Energy Lithium-Ion Batteries

Ting Liu ¹, Xuemei Hu ¹, Yadong Zhang ¹, Ting He ¹, Yunxiang Guo ² and Junqiang Qiao ^{1,*}

¹ Gansu Natural Energy Research Institute, International Solar Energy Center, Lanzhou 730046, China; ting.liu@gsas.ac.cn (T.L.); xmhu@gsas.ac.cn (X.H.); zhangyadong@gneri.com.cn (Y.Z.); changyong@lzpcc.edu.cn (T.H.)

² School of Materials and Energy, Lanzhou University, Lanzhou 730000, China; 220220900091@lzu.edu.cn

* Correspondence: qiao@gsas.ac.cn; Tel.: +86-0931-8386604

Abstract: Cathodes undergo unavoidable lithium loss due to the formation of a solid electrolyte interface (SEI), which seriously affects the energy density of lithium iron phosphate (LFP) batteries. To compensate for the initial capacity loss, we introduced an NiCo-Li₂Se nanocomposite to an LFP battery system to act as a competitive cathode prelithiation additive. Benefiting from its zero gas-emissions, ambient stability, high irreversible capacity, low delithiation potential, and good compatibility with carbonate-based electrolytes, the NiCo-Li₂Se additive based on the chemical conversion reaction effectively offset the initial lithium loss. As a result, with 10 wt% addition, the initial charge capacity of the Li || LFP half-cell was improved by 34 mA h g⁻¹. The Gra || LFP-Li₂Se full-cell released an initial discharge specific capacity of 159.7 mA h g⁻¹, which increased by 18% compared with the Gra || LFP full-cell, resulting in improved cycling stability. In addition, COMSOL Multiphysics simulation was applied to verify the function of the NiCo-Li₂Se additive, and pouch cells were assembled to explore its potential in large-scale industrial application. This work provides a meaningful research direction for the design of a prelithiation additive for LFP cells.

Keywords: lithium-ion batteries; cathode prelithiation; Li₂Se; initial capacity loss; chemical conversion reaction



Academic Editor: Marco Giorgetti

Received: 12 December 2024

Revised: 9 January 2025

Accepted: 10 January 2025

Published: 11 February 2025

Citation: Liu, T.; Hu, X.; Zhang, Y.; He, T.; Guo, Y.; Qiao, J. Bimetal/Li₂Se Nanocomposite as Cathode

Prelithiation Additive for Sustainable High-Energy Lithium-Ion Batteries.

Batteries **2025**, *11*, 74. <https://doi.org/10.3390/batteries11020074>

Copyright: © 2025 by the authors. Licensee MDPI, Basel, Switzerland. This article is an open access article distributed under the terms and conditions of the Creative Commons Attribution (CC BY) license (<https://creativecommons.org/licenses/by/4.0/>).

1. Introduction

With the rapid development of wind energy, photovoltaics, and other renewable energy power industries, the problem of abandoning light and wind is becoming more and more serious. Energy storage batteries can store energy from a photovoltaic power generation system and supply power to a load when there is insufficient sunshine or during nighttime or emergency states [1,2]. Among the different energy storage batteries, lithium iron phosphate (LiFePO₄) batteries have large input and output power, a wide operating temperature range, a long service life (2000 times), and no memory effect and are constructed using abundant raw material reserves [3]. The volume specific energy of LiFePO₄ is 4~5 times that of the traditional lead-acid battery, which can greatly reduce the space occupied by the battery, making it the best choice for the practical application of photovoltaic energy storage batteries [4,5].

However, during the initial charging process of lithium-ion batteries, the organic electrolyte reduces and decomposes on the anode surface, forming a solid electrolyte interface (SEI) layer which permanently consumes a large amount of cathodic lithium (5~20%), resulting in a low initial Coulombic efficiency (ICE), and finally, reducing the

energy density of the entire battery [6–8]. In order to minimize the lithium loss during SEI formation, prelithiation technology has emerged, including chemical prelithiation [9,10], electrochemical prelithiation [11,12], and the introduction of prelithiation additives to electrodes [13–15]. These approaches compensate for the Li^+ loss by introducing extra active Li^+ into the system. Among the above strategies, introducing prelithiation additives to the battery system, especially to the cathode, has drawn the most attention due to its facile operation, high safety, and good practicality [16].

Ideal cathode prelithiation additives should be equipped with a series of properties, including a high supply capacity of Li, appropriate extraction potential of Li, and favorable compatibility with the battery system [17]. In terms of typical cathode additives, there are three main categories according to the prelithiation mechanism: first, lithium-rich compounds, such as Li_2NiO_2 , Li_2MoO_3 , and Li_2CuO_2 [18–20], exhibiting stability in relation to water/oxygen but low capacities ($300\text{--}400 \text{ mA h g}^{-1}$), which limits the Li compensation effect of the initial cycle; second, sacrificial lithium salts, such as Li_5FeO_4 and $\text{Li}_2\text{C}_2\text{O}_4$ [21,22], producing a relatively high specific capacity but undesired gasses or residual delithiated products after the first charging process; and third, binary compounds and their derivates based on the conversation reaction, including Li_2O , Li_2O_2 , Li_2S , Li_3N , LiF , Li_3P , and the corresponding metal complex [23–29].

Due to their high specific capacities, increasing attention has been paid to binary compounds and their conversation-type derivates. However, additives like Li_2O , Li_2O_2 , and Li_3N release oxygen (O_2) and nitrogen (N_2) gases during delithiation; this phenomenon could be minimized by adding metal nanoparticles like Co, Ni, and Fe [23]. As for Li_2S , it possesses a high theoretical capacity of 1167 mA h g^{-1} , while its delithiation product S exhibits a poor electronic conductivity of $5 \times 10^{-30} \text{ S}\cdot\text{m}^{-1}$ [27,30]. To make Li_2S a feasible cathode prelithiation agent, nanocomposites such as $\text{Li}_2\text{S}/\text{super-activated carbon}$ [27] and $\text{Li}_2\text{S}/\text{KB/PVP}$ [31] have been reported and applied in graphite || LiFePO_4 full cells with 11.7% improved discharge capacity. By contrast, the Li_2S system was found to be incompatible with carbonate-based electrolytes for conventional lithium-ion batteries; thus, finding a suitable cathode pre-lithiation additive is still a great challenge.

Selenium (Se), as the congener of S, has been explored as an alternative cathode material for next-generation lithium batteries. The lithiation product Li_2Se can be used as a cathode prelithiation material as Li_2S . It exhibits the following characteristics: (1) Li_2Se releases a theoretical volumetric specific capacity of $1659 \text{ mA h cm}^{-3}$; (2) Li_2Se shows an appropriate working voltage window; (3) in contrast to Li_2S , there is no incompatibility problem between Li_2Se and carbonate electrolytes; and (4) the relative high conductivity ($1 \times 10^{-5} \text{ S}\cdot\text{m}^{-1}$) and high density of Li_2Se are advantageous for the electrochemical performance of batteries [32–34]. Under these conditions, Li_2Se can serve as a competitive cathode prelithiation material. Nevertheless, there are two important problems that need to be solved before its application: the poor reaction kinetics of Li_2Se particles in carbonate-based electrolytes and their instability under the ambient fabrication condition.

Herein, we propose a rational structure and component design to synthesize bimetals/ Li_2Se nanocomposites ($\text{NiCo-Li}_2\text{Se}$) by a chemical conversation reaction between metallic lithium and metal selenides derived from metal–organic frameworks (MOFs). The high irreversible capacity, low delithiation potential, and good compatibility with the commercial carbonate-based electrolyte demarcate $\text{NiCo-Li}_2\text{Se}$ as a competitive cathode prelithiation material. As a result, the $\text{NiCo-Li}_2\text{Se}$ nanocomposite possesses a high pre-lithiation capacity (546 mA h g^{-1}) but a low discharge specific capacity (27 mA h g^{-1}). With 10 wt% addition of the $\text{NiCo-Li}_2\text{Se}$ additive, the initial charge capacity of the $\text{Li}||\text{LFP}$ half-cell was improved by 34 mA h g^{-1} , and the initial discharge specific capacity of the graphite || LFP full-cell was enhanced from 115.2 to 152 mA h g^{-1} . In addition, a pouch

cell was assembled to demonstrate the potential of this new type of prelithiation material in large-scale applications. This work affirms the applied potential of Li₂Se based on the conversion reaction, and it provides a meaningful design idea for prelithiation strategies to compensate for the loss of energy density in LFP cells.

2. Materials and Methods

2.1. Synthesis of the NiCoSe₂ Polyhedron Precursor

According to the reported method [35], 4 mmol of Co(NO₃)₂·6H₂O and 4 mmol of Ni(NO₃)₂·6H₂O (with the molar ratio of Co/Ni as 1: 1) were dissolved in 200 mL of methyl alcohol, which was labeled as solution A. Then, 40 mmol of 2-methylimidazole (C₄H₆N₂) was dissolved in 200 mL of methyl alcohol to form solution B. Next, solution A was slowly poured into solution B, and the mixture was magnetic stirred for 20 min. After standing for 24 h at room temperature, the obtained precipitates were collected via centrifugation. After being washed three times with methanol and vacuum dried at 70 °C overnight, the NiCo-ZIF purple powder was obtained. Subsequently, the mixture of NiCo-ZIF and Se powder with certain mass ratio was placed in a high-temperature tube furnace under Ar atmosphere. Finally, after being annealed at 800 °C for 4 h (heating rate of 5 °C min⁻¹), the mixture was successfully transformed into a transition metal selenide, namely, NiCoSe₂.

2.2. Synthesis of the NiCo-Li₂Se Additive

The NiCo-Li₂Se nanocomposite additive was synthesized using the lithium foil and MOFs-derived metal selenides (NiCoSe₂) through a chemical conversion reaction. The preparation operations were performed in an Argon-filled glovebox in which the concentrations of moisture and oxygen were both below 0.1 ppm. To synthesize the NiCo-Li₂Se additive, molten lithium foil (12 mmol, China Energy Lithium Co., Ltd., Tianjin, China) and NiCoSe₂ (4 mmol) were mixed at 180 °C, followed by mechanical stirring for 30 minutes. Then, the heating temperature was raised to 200 °C, and the reaction was allowed to run for 2 h under continuous stirring.

2.3. Preparation of the LFP Cathodes with and Without NiCo-Li₂Se Additive

The slurry of the LiFePO₄ (LFP) electrode with NiCo-Li₂Se additive was produced under ambient condition. The modified LFP cathode slurry was made up of 10% NiCo-Li₂Se prelithiation material, 70% commercial LFP powder (MTI Corporation, Shenzhen, China), 10% Super P carbon, 10% polyvinylidene fluoride (PVDF) binder, and a sufficient quantity of N-methyl-2-pyrrolidone (NMP) solvents. After being dried in vacuum at 120 °C, the LFP cathodes with an average mass loading of 2.5 mg cm⁻² were obtained. The pristine LFP slurry was composed of 80% LFP powder, 10% Super P, and 10% PVDF in NMP solvents. The other operation processes were the same as those of the LFP cathodes with NiCo-Li₂Se additive.

2.4. Preparation of Pure NiCoSe₂ Cathode and Commercial Graphite Anode

For the fabrication of the pure NiCoSe₂ electrode, 70% active materials, 20% Super P, 10% PVDF binder, and NMP solvents were used to make the slurry. The final NiCoSe₂ electrodes were created with an average mass loading of 1.5 mg cm⁻². For the fabrication of the graphite anodes, a homogeneous slurry was made by mixing commercial graphite powder, Super P, and PVDF with a weight ratio of 90:5:5. The slurry was cast on Cu foil and dried before being cut into disks (13 mm). The obtained electrodes demonstrated an areal mass loading of graphite carbon of about 3 mg cm⁻².

2.5. Electrochemical Measurements

To conduct an electrochemical investigation of the above electrodes, CR2032 coin cells were assembled in an Ar-filled glovebox. In each coin cell, the lithium foil acted as a counter electrode as well as a reference electrode, the Celgard 2500 membrane acted as the separator, and 1.0 M LiPF₆ in a mixture of ethylene carbonate (EC), dimethyl carbonate (DMC), and ethyl methyl carbonate (EMC) (1: 1: 1 Vol%) acted as the electrolyte. Each cell consumed 80 μ L of the electrolyte. The specific capacities of the cathodes were calculated according to the mass of LFP powder.

The galvanostatic charge/discharge performance was assessed using a Neware Battery Tester. The charge/discharge curves of the LFP half cells were operated within a potential range of 2.5~3.8 V vs. Li/Li⁺ at 0.1 C for the first two cycles and 1 C upon cycling (1 C = 170 mA h g⁻¹). For comparison, the cells with NiCoSe₂ cathodes and Li foil anodes were operated within the potential range of 2.0~4.0 V at a current density of 100 mA g⁻¹. The full cells were assembled with a N/P ratio of 1.2 and cycled at 0.1 C three times for activation and at 1 C for the following cycles within a potential range of 2.0~4.0 V. With the electrochemical workstation (Chenhua CHI760E, Shanghai, China), cyclic voltammetry (CV) characterization was performed at a scan rate of 0.1 mV s⁻¹, and a series of electrochemical impedance spectra were measured within a frequency range of 100 kHz to 0.1 Hz.

2.6. Characterization

The structure of the samples was characterized using XRD patterns obtained with a Bruker-D8 diffractometer (Bruker, Billerica, MA, USA) in the range of 10°~80°. The SEM and EDX elemental mapping characterizations were performed on a field emission scanning electron microscope (FESEM, Hitachi S-4800, Hitachi, Japan), and the TEM and HRTEM images were acquired from Tecnai G2 F30 (Thermo Fisher, Waltham, MA, USA). X-ray photoelectron spectroscopy (XPS, Thermo ESCALAB 250XI, Thermo Fisher, USA) was employed to estimate the valence state of precursors and the structure evolution of the NiCo-Li₂Se during the charging/discharging processes. To minimize the influence of the residue in the electrolyte, before XPS measurements, the cycled LFP cathode with NiCo-Li₂Se additive was washed with DMC solvents and allowed to dry overnight under vacuum at room temperature. Electrochemical measurements were carried out on a CHI760E electrochemical workstation.

2.7. COMSOL Operation

A half-cell model and a full-cell model were constructed in the COMSOL Multiphysics software, including the electrodes and separators. In the half-cell model, the battery cathode particles were divided into two substances: the large ball was the LPF powder, and the small ball was the lithium additive. Then, we used the lithium-ion battery module to build the model. After setting the parameters in the corresponding area that were consistent with the experimental material, a current of 1A was applied to the positive electrode for charge and discharge. Finally, the electrochemical parameters were obtained.

3. Results and Discussion

3.1. Characterization of the NiCo-Li₂Se Additive

The NiCo-Li₂Se additive was synthesized through a chemical prelithiation approach between NiCoSe₂ powder and Li-metal (Figure 1a). First, purple NiCo-ZIF powder was prepared by the self-assembly of metal centers and organic ligands, whose XRD pattern is provided in Figure S1a. Afterwards, certain amount of Se powder was thoroughly blended with NiCo-ZIF, whereby the mixture transformed into NiCoSe₂ after an annealing treatment. Finally, the NiCo-Li₂Se was acquired by initiating the chemical conversion

reaction between bimetallic selenide and molten lithium metal. The phase and crystallinity of the samples were confirmed by XRD. As shown in Figure 1e, for the XRD pattern of NiCoSe₂, the diffraction peaks located at 33, 44.5, 50, 59.6, 61, and 69 could be assigned to hexagonal NiCoSe₂ (JCPDS 65-7038), demonstrating the successful synthesis of NiCoSe₂. The pattern of NiCo-Li₂Se was almost the same as that of NiCoSe₂, resulting from the limited conversion amount of Li₂Se, whose standard peaks can be clearly seen in the enlarge XRD pattern of NiCo-Li₂Se in Figure S1b.

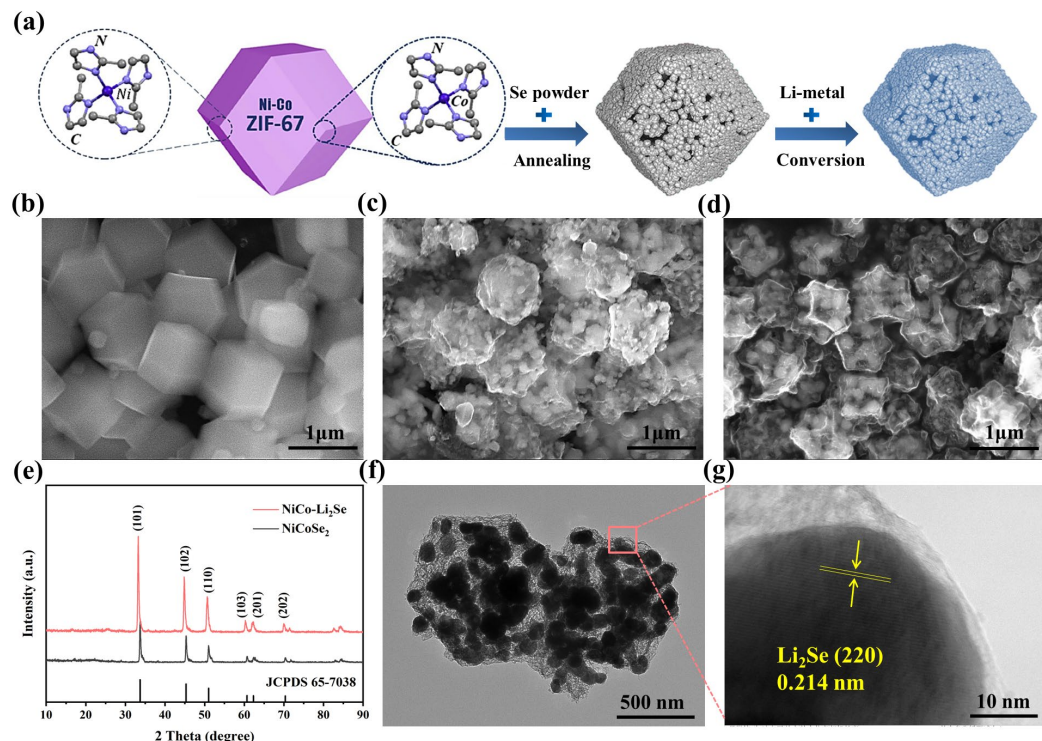


Figure 1. (a) Schematic for the formation of NiCoSe₂ and NiCo-Li₂Se nanocomposite; (b–d) SEM images of NiCo-ZIF, NiCoSe₂ and NiCo-Li₂Se nanocomposite, respectively; (e) XRD patterns of NiCoSe₂ and NiCo-Li₂Se; (f,g) TEM and HRTEM image of the NiCo-Li₂Se nanocomposite.

Figure 1b–d display the SEM images of the NiCo-ZIF, NiCoSe₂, and NiCo-Li₂Se, respectively. It can be seen that the polyhedral morphology of NiCo-ZIF was perfectly maintained after annealing and the integration of Li-metal, except that the NiCoSe₂ and NiCo-Li₂Se nanocomposite had rough surfaces and plentiful nanoparticles inside. In addition, with the increasing degree of selenization, the number and size of the embedded nanoparticles also increased (Figure S2). The TEM image of NiCo-Li₂Se in Figure 1f shows that particles with 50~100 nm size were evenly distributed on polyhedrons, which is in agreement with the SEM image in Figure 1d. This relatively large particle size indicated the presence of NiCo-Li₂Se with a low practicable surface area, which greatly improved the stability of the additive under ambient conditions. As for the HRTEM image, Figure 1g clearly shows a series of lattice fringes with an inter planar space of 0.214 nm; this was associated with the (220) plane of Li₂Se, which further confirmed the successful fabrication of Li₂Se. Moreover, the outer coating layer derived from ZIF-based carbon skeleton could optimize the ambient stability of Li₂Se, strengthening the ability of Li₂Se to serve as an air-stable cathode additive.

3.2. The Evolution of NiCo-Li₂Se Additive During Electrochemical Processes

To explore the prelithiation mechanism of the NiCo-Li₂Se additive with regard to its structure, the evolution of Se 3d and N 1s peaks, characterized by XPS spectra, was

examined, as shown in Figure 2. In the schematic illustration of the reaction process of LFP with the NiCo-Li₂Se additive (Figure 2a), the NiCoSe₂ powder transformed into NiCo-Li₂Se via a chemical conversion reaction with molten lithium. Then, the as-synthesized NiCo-Li₂Se additive was introduced and applied to the LFP cathode using the common slurry casting method. During the first charging process, NiCo-Li₂Se released all of the lithium ions inside, which effectively compensated for the lithium loss in the cathode.

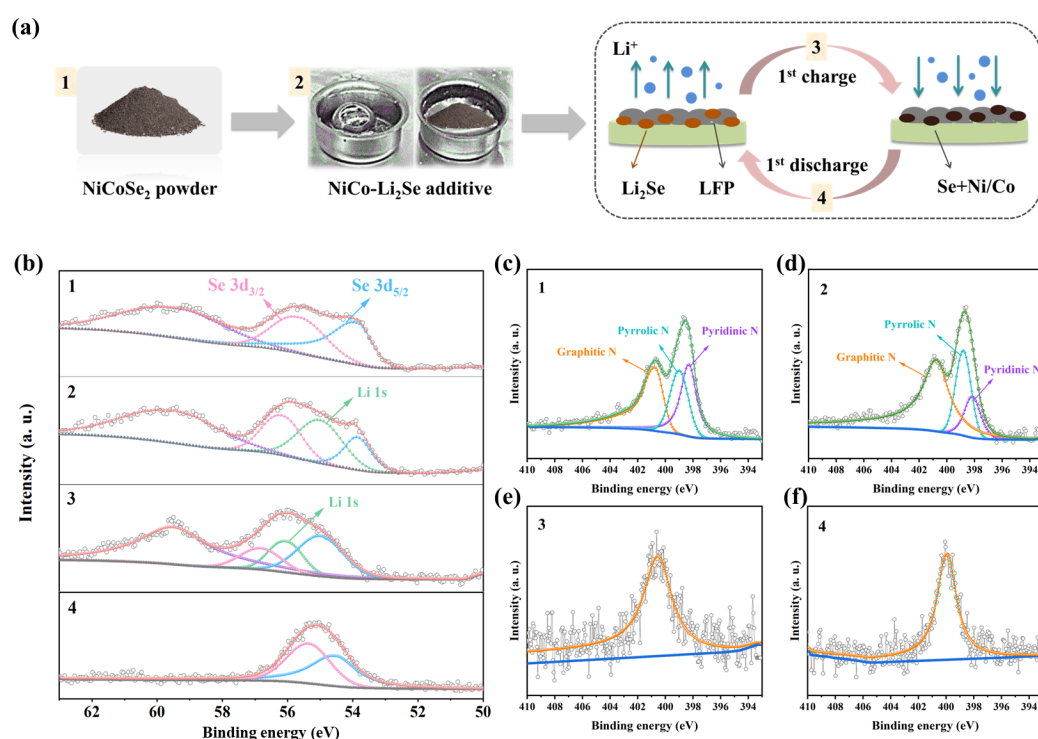


Figure 2. Prelithiation mechanism of NiCo-Li₂Se additive. (a) Schematic illustration of the reaction process for LFP with a NiCo-Li₂Se cathode; (b) Refined XPS spectra of Se 3d peaks in different states; (c–f) Refined XPS spectra of N 1s peaks in different states.

To examine the capability of the NiCo-Li₂Se cathode prelithiation additive, an initial charging/discharging curve was established in a half cell with a Li anode. As shown in Figure S3, at a current density of 100 mA g⁻¹ in the potential range of 2.0~4.0 V, the NiCo-Li₂Se cathode displayed a charge specific capacity of 546 mA h g⁻¹, higher than that of some reported prelithiation additives [18,20]. There was a long slope voltage plateau within the charging potential range of 3.0~4.0 V, which corresponded to the delithiation process of the NiCo-Li₂Se, indicating its application potential as a commercial LFP cathode. Moreover, the NiCo-Li₂Se only delivered a discharge specific capacity of 27 mA h g⁻¹ above the cutoff potential of 2.0 V. As a result, the NiCo-Li₂Se nanocomposite was found to be capable of releasing a specific capacity of 519 mA h g⁻¹ in the first cycle, making it a remarkably high “donor” of lithium ions. The above mentioned characteristics of the NiCo-Li₂Se, including high delithiation capacity but low lithiation capacity, feasible delithiation voltage, and good compatibility with carbonate-based electrolyte, confirm its potential to serve as a cathode prelithiation additive.

In terms of the evolution of elemental Se during the chemical and electrochemical processes, XPS spectra were employed, as exhibited in Figure 2b. From top to bottom: State 1 represents the condition of Se in the NiCoSe₂ powder, in which the main peaks of Se 3d_{3/2} and Se 3d_{5/2} were centered at ~53.9 and ~56.0 eV, which could be attributed to metallic selenium; Next, state 2 represents the fresh LFP electrode with fresh NiCo-Li₂Se. Except for the characteristic peaks of Se 3d_{3/2} and Se 3d_{5/2}, there was a peak of Li 1s located

at ~ 55.2 eV, indicating the successful introduction of metallic lithium and the presence of Li_2Se . In State 3, i.e., the fully charged state of the LFP electrode with the $\text{NiCo-Li}_2\text{Se}$ additive, the peaks belonging to Se 3d and Li 1s were all left-shifted to higher binding energies, i.e., about ~ 0.8 eV, which showed that the delithiation process of the $\text{NiCo-Li}_2\text{Se}$ additive brought about obvious changes to the integration mode between Se and the NiCo-ZIF derived carbon polyhedra; Finally, with the cell being discharged to 2.0 V in State 4, the XPS spectrum of Se 3d exhibited almost the same curve as that of NiCoSe_2 , which demonstrated that the delithiation product of $\text{NiCo-Li}_2\text{Se}$ was not only stable but also no longer consuming active lithium ions at the discharge cut-off voltage of 2.0 V.

The above-mentioned results are in agreement with the Se 3p XPS spectra in Figure S4, in the State 3 (fully charged) condition. The Se $3p_{1/2}$ and $3p_{3/2}$ peaks were located at ~ 171.1 eV and ~ 165.8 eV, indicating the delithiation of Li_2Se to Se. Upon being discharged to 2.0 V, the Se 3p spectra of the nanocomposite could roughly maintain the patterns of the Se $3p_{1/2}$ and $3p_{3/2}$ peaks, which further proved the stability of $\text{NiCo-Li}_2\text{Se}$. As for the N1s spectra (Figure 2c–f), it presented pyridinic, pyrrolic, and graphitic three types of N in States 1 and 2; the subtle differences were the decrease in pyridinic-N and increase in pyrrolic-N after the reaction between metallic Li and NiCoSe_2 to form $\text{NiCo-Li}_2\text{Se}$. When it comes to States 3 and 4 in Figure 2e,f, the graphitic-N assumed a leading position, resulting from the participation of $\text{NiCo-Li}_2\text{Se}$ in the initial charge–discharge reaction. Based on the results of our XPS survey, the C 1s and Co 2p spectra of different samples are presented in Figure S5, Figure S6, and Figure S7, respectively. In addition, the parameters used in the fitting of the high resolution XPS spectra are presented in Table S1 in the Supporting Information.

3.3. Electrochemical Performance of the LFP Cathode with the $\text{NiCo-Li}_2\text{Se}$ Additive

To explore the prelithiation mechanism of the $\text{NiCo-Li}_2\text{Se}$ additive, the initial charge/discharge profiles, CV tests, and a COMSOL theoretical simulation were conducted, as presented in Figure 3. The initial galvanostatic charge/discharge profiles of the pristine LFP and LFP with the $\text{NiCo-Li}_2\text{Se}$ additive are shown in Figure 3a. The pristine LFP displayed a charge capacity of $169.6 \text{ mA h g}^{-1}$ and a reversible discharge capacity of $156.8 \text{ mA h g}^{-1}$, which showed an ICE value of 92.5%. In comparison, owing to the extra active Li provided by the $\text{NiCo-Li}_2\text{Se}$ nanocomposite, the LFP electrode with 10% prelithiation additive delivered a high charge specific capacity of 205 mA h g^{-1} , a raised reversible discharge capacity of $169.2 \text{ mA h g}^{-1}$, and an ICE of 82.5%, calculated according to the total weight of LFP and $\text{NiCo-Li}_2\text{Se}$. In particular, the movements in the discharge curves of the $\text{Li} \parallel \text{LFP}$ and $\text{Li} \parallel \text{LFP} + \text{NiCo-Li}_2\text{Se}$ cells basically stayed the same, and there was no new slope in the whole discharge process, revealing that the lithiation of $\text{NiCo-Li}_2\text{Se}$ did not happen from 4.0 to 2.0 V. This observation was in accordance with the following CV results.

The effect of the $\text{NiCo-Li}_2\text{Se}$ additive on the electrochemical behavior of the $\text{Li} \parallel \text{LFP}$ half cells was investigated by CV testing. With a sweep rate of 0.1 mV s^{-1} in a voltage range of $2.0 \sim 4.0$ V, the first five laps of the CV curves for LFP with $\text{NiCo-Li}_2\text{Se}$ are shown in Figure 3b. With the addition of 10 wt% $\text{NiCo-Li}_2\text{Se}$, a new small oxidation peak at ~ 3.0 V was observed in the $\text{Li} \parallel \text{LFP-Li}_2\text{Se}$ cell (Figure S8) in the first cycle (black line), which could be assigned to the delithiation process of Li_2Se [32]. It is noteworthy that the related lithiation peak was not observed within the discharge cut-off voltage (2.0 V) of the LFP cells, which illustrates the electrochemical reaction of $\text{NiCo-Li}_2\text{Se}$ within the working voltage range was totally irreversible.

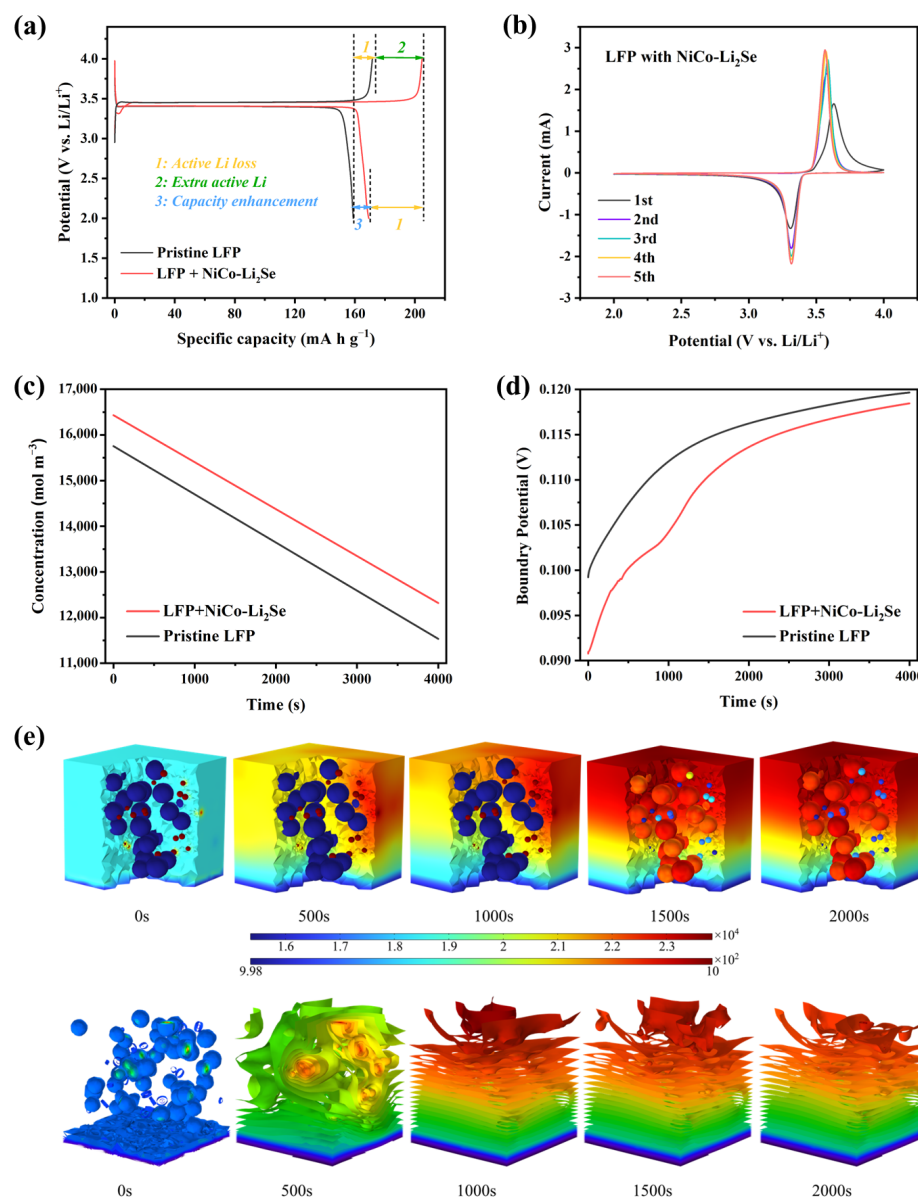


Figure 3. (a) The initial charge/discharge profiles of the pristine LFP and Li || LFP-Li₂Se cell in the 2.0~4.0 V voltage range; (b) The first five CV curves for the Li || LFP cells with NiCo-Li₂Se additive at a scan rate of 0.1 mV s⁻¹; (c) The simulated average concentration of positive electrodes during the first charging process; (d) The simulated electrode potential to earth (boundary potential) of different cells during the first charging process; (e) The simulation results using COMSOL Multiphysics provides the lithium ion concentration distribution within the LFP electrode with NiCo-Li₂Se additive.

Furthermore, to verify the improvement to the LFP cathode through the addition of NiCo-Li₂Se, we simulated the Li⁺ concentration distribution in a modified electrode using the finite element method in COMSOL Multiphysics as a function of the density of the cathode material and the concentration of the electrolyte. As demonstrated in Figure 3e, the whole time-changing process (0~2000 s) refers to the first charging process of the LFP half-cell, and the pellets and particles represent the LiFePO₄ and NiCo-Li₂Se additive, respectively. It is worth noting that with the participation of Li₂Se particles, the concentration color changed from dark red to blue, indicating the release and de-intercalation of Li⁺. Moreover, the corresponding isosurface contour diagrams mainly consisted of orange and green, compared with the red-yellow-blue color layout of the LFP battery system without additive (see Figure S10). This demonstrated that the introduction

of the lithium additive particles caused an increase in the local Li^+ concentration at this site and the presence of more uniform diffusion paths. Furthermore, during the same time period, the variation of the average concentration for the positive electrode and electrode potential to earth (boundary potential) were also simulated, as shown in Figure 3c,d. As a result, the LFP with the NiCo-Li₂Se additive displayed a higher average concentration and a lower boundary potential compared with the pristine LFP electrode. As for the reason, the Li^+ concentration increased after prelithiation; then, the electronegativity of the positive material lattice decreased, resulting in a decrease in potential. This observation is consistent with the isosurface contour diagrams in Figure 3e.

To assess the prelithiation effectiveness of the NiCo-Li₂Se nanocomposite in an LFP battery system, we further developed LFP cathodes with certain amounts of NiCo-Li₂Se; the corresponding electrochemical performance is shown in Figure 4. In Figure 4a, the initial charge–discharge profiles of the parallel-contrast Li||LFP cells were measured at 0.1C (1 C = 170 mA h g⁻¹). It is worth noting that with the continuous addition of the additive, the open-circuit voltage (OCV) of cells was reduced and the potential slope below 3.5 V was gradually right-shifted. In addition, the half cells with 5% and 10% additive released initial charge capacities of 180 and 205 mA h g⁻¹, which was, respectively, 9 mA h g⁻¹ and 34 mA h g⁻¹ higher than that of the pristine LFP cells.

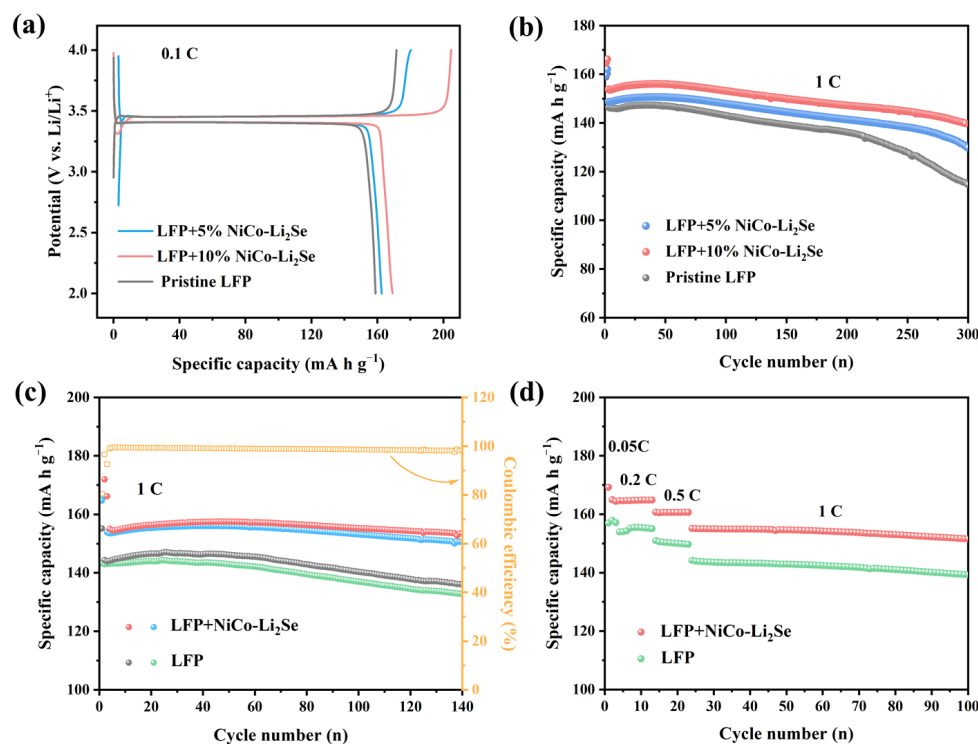


Figure 4. Electrochemical properties of the Li||LFP half cells with and without NiCo-Li₂Se additive. (a,b) The initial charge/discharge profiles and cycling performance of the pristine LFP and cells with 5 wt% and 10 wt% NiCo-Li₂Se prelithiation additive at 0.1 C and 1 C; (c,d) The cycling performance and rate performance of contrastive Li||LFP as well as the Li||LFP + NiCo-Li₂Se half cells.

The capacity enhancement of the LFP cathode with NiCo-Li₂Se additive was not the same as that of the pure NiCo-Li₂Se cathode; this may have resulted from the changed carbon content in the electrodes. Figure 4b contrasts the cycling performance of the Li||LFP cells with 5% additive, 10% additive, and without additive at 1C (1C= 170 mA h g⁻¹), in which the LFP with 10% NiCo-Li₂Se additive exhibited a discharge capacity of 140 mA h g⁻¹ over 300 cycles. Compared with the pristine Li||LFP cell, there was an apparent capacity improvement as high as 22%. The cycling stability is further displayed

in Figure S11. As for the Coulombic efficiency, the LFP with 10% NiCo-Li₂Se additive exhibited a moderate value of 94.6% after 300 cycles. The SEM images of the electrode surface for the LFP with NiCo-Li₂Se after being cycled for 300 times are shown in Figure S12, further proving the stability of the electrode. The above results indicate that the NiCo-Li₂Se nanocomposite took part in the initial charge process and provided extra lithium ions to the LFP battery system, leading to the improved specific capacities and long-term cycling stability of the LFP with NiCo-Li₂Se additive.

In consideration of the better characteristics of the LFP with 10% NiCo-Li₂Se additive, further electrochemical measurements and a performance comparison were carried out, comparing the 10% sample and the pristine LFP. Regarding the cycling performance in Figure 4c, the positive effect of the prelithiation additive was confirmed once again by the significantly increased specific capacities during the whole 140 cycles. The final 140th Coulombic efficiency reached 98.2% (1.7% higher than that of the pristine LFP cathode). In addition, regarding the rate performance of the different cell systems in Figure 4d, after being activated at 0.05 C for two cycles, the cells were tested first at 0.2 C, then at 0.5 C, and finally at 1 C. The results revealed that the addition of NiCo-Li₂Se had a non-negligible effect on the rate capability of LFP electrode. Also, the impact of this new additive on the cathode was proved through the electrochemical impedance spectrum (EIS) results. The related EIS plots of different Li || LFP cells after a certain number of cycles are illustrated in Figure S13. In the high-frequency region, the semicircle corresponds to R_{SEI} , namely, the interfacial charge-transfer impedance, whose value was slightly increased after the addition of the NiCo-Li₂Se nanocomposite; while in the low-frequency region, the ionic diffusion impedance could be inferred from the inclination degree of slope, which was also confirmed by the Warburg coefficient (σ). After the 10th cycle, the plot of the LFP cathode with additive presented obviously decreased interfacial impedance, indicating that the electron and ion transfer had accelerated; this was helpful for the kinetics of subsequent electrode reaction. It was noted that after introducing NiCo-Li₂Se additive, the total resistance value was larger than that of the pristine LFP cell; this could be attributed to the dissolution and shutting effect of the polyselenides. As reported, after polallowing the yselenides to react with the electrolytes, the products were likely adsorbed on the electrode's surface, hindering the electron and ion transportation and offering increased resistance [36].

3.4. Electrochemical Performance of NiCo-Li₂Se Additive in Full Cells

To study the influence of the NiCo-Li₂Se additive on the Li storage electrochemistry, Gra || LFP-Li₂Se full cells were further assembled. Their performance was almost the same as that achieved by the LFP half cells. Figure 5a displays the initial charge/discharge curves of the full cells at 0.1 C in the voltage range of 2.0~4.0 V vs. Li/Li⁺, in which the Gra || LFP and the Gra || LFP-Li₂Se full cells released an initial discharge specific capacity of 135.3 mA h g⁻¹ and 159.7 mA h g⁻¹, respectively. After the addition of NiCo-Li₂Se, the specific capacity increased by 18%, demonstrating that this new prelithiation additive was capable of compensating for the lithium loss during the initial cycle by emitting sufficient lithium ions. After being activated at 0.1 C for the first two cycles, the cycling performances of the two kinds of full cells were tested at a current density of 1 C; the profiles are presented in Figure 5b. It is worth noting that the Gra || LFP-Li₂Se full cell revealed superior cycling stability (70% capacity retention) compared to the Gra || LFP cell after 100 cycles. Also, the Gra || LFP-Li₂Se full cell presented higher initial CE and an average CE value compared to the Gra || LFP cell. During the initial cycle, the NiCo-Li₂Se nanocomposite played the role of a lithium reservoir, and it liberated additional lithium ions to compensate for the inevitably consumed active lithium.

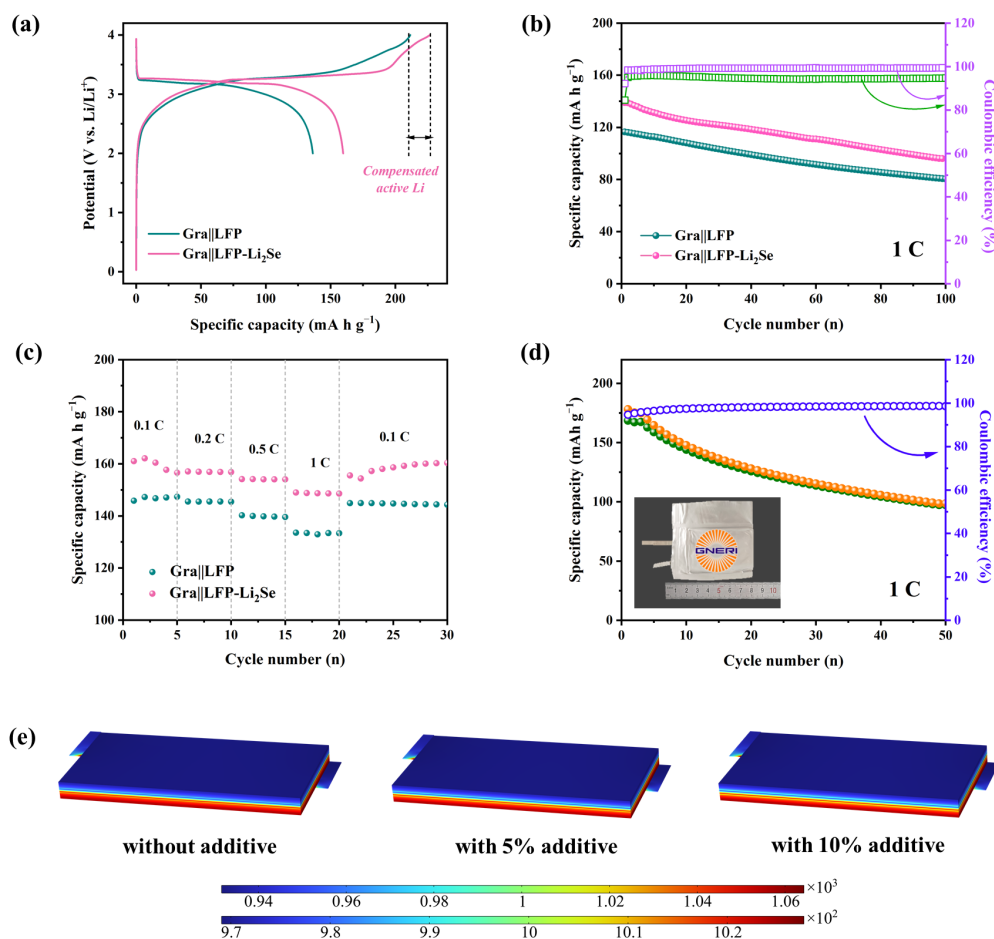


Figure 5. Electrochemical properties of the full cells with and without NiCo-Li₂Se additive. (a) The initial charge/discharge curves of the contrastive full cells at 0.1 C (activated for the first two cycles); (b) The cycling performance of the contrastive full cells at 1 C; (c) The rate performance of the full cells; (d) The cycling performance of the graphite || LFP-Li₂Se pouch cell (the inserted optical image is the as-assembled pouch cell); (e) The simulation results using COMSOL Multiphysics provided the lithium ion concentration distribution within the graphite || LFP pouch cells.

To investigate the rate performance of the contrastive full cells, the Gra || LFP and the Gra || LFP-Li₂Se cells were tested at 0.1 C, 0.2 C, 0.5 C, and 1 C each for 5 cycles. When set back to 0.1 C, the specific capacities were well recovered and maintained as high as those at the beginning (Figure 5c). In detail, the obtained Gra || LFP-Li₂Se full cell showed an average high reversible capacity of 148.8 mA h g⁻¹ at 1 C, whereas the Gra || LFP cell delivered an average reversible capacity of 134 mA h g⁻¹. Furthermore, the graphite || LFP-Li₂Se pouch cell was assembled to evaluate the potential of NiCo-Li₂Se as a prelithiation additive in industrial applications (Figure 5d). The obtained pouch cell exhibited a relatively high reversible capacity of 101.6 mA h g⁻¹ at 1 C after 50 cycles with an average Coulombic efficiency of 98.6%. In addition, we simulated the Li⁺ concentration distribution in different pouch cells using the COMSOL Multiphysics. As shown in Figure 5e, even though the variation in the pouch cells was not as obvious as that of half cells, the slight change of Li⁺ concentration distribution could be captured after the introduction of the NiCo-Li₂Se additive. It is noteworthy that with a 10% addition of NiCo-Li₂Se nanocomposites, the Li⁺ concentration distribution in the pouch cell was the most uniform. The boundary potential and state of charge (SOC) performance of different pouch cells are exhibited in Figure S14a,b, in which the cell with 10% addition of NiCo-Li₂Se demonstrated the lowest

boundary potential and the highest SOC value during the same time period, demonstrating its improved Li⁺ concentration and battery lifespan.

4. Conclusions

In summary, a NiCo-Li₂Se nanocomposite was synthesized and introduced to the LFP cathode to compensate for the active lithium loss in the first cycle. On this basis, the corresponding prelithiation mechanism was investigated. Basically, this new type of cathode additive did not release gas during the delithiation processes, and it was stable under ambient condition. Importantly, the high irreversible capacity, low delithiation potential, along with good compatibility with the commercial carbonate-based electrolyte, revealed NiCo-Li₂Se to be a competitive cathode prelithiation material. The NiCo-Li₂Se modified graphite || LFP full cell displayed an enhanced initial discharge specific capacity by 18%, together with improved cycling stability. The results in this work indicate that NiCo-Li₂Se maybe a competitive cathode prelithiation additive for high-energy LFP batteries, with prospects for large-scale energy storage applications.

Supplementary Materials: The following supporting information can be downloaded at: <https://www.mdpi.com/article/10.3390/batteries11020074/s1>, Figure S1: (a) XRD pattern of NiCo-ZIF precursor; (b) enlarge image of XRD pattern for NiCo-Li₂Se nanocomposite; Figure S2: The SEM images of NiCoSe₂ with different degree of selenization; Figure S3: The initial charge/discharge curve of the Li || NiCo-Li₂Se cell in the range of 2.0~4.0 V; Figure S4: The refined XPS spectra of Se 3p peaks of different states; Figure S5: The XPS survey scan results of different samples; Figure S6: The XPS spectra of C 1s in different samples; Figure S7: The XPS spectra of Co 2p in different samples; Figure S8: The enlarge image of CV profiles for LFP with NiCo-Li₂Se additive; Figure S9: CV profiles of the pristine LiFePO₄ electrode; Figure S10: The simulation results using COMSOL Multiphysics provides the lithium ion concentration distribution within the LFP electrode without additive; Figure S11: The corresponding Coulombic efficiency during cycling processes of pristine LFP and cells with 5 wt % and 10 wt % NiCo-Li₂Se additive at 1 C; Figure S12: The SEM images of the LFP-NiCo-Li₂Se electrode surface after cycling for 300 times; Figure S13: The related EIS plots of different Li || LFP cells (a) after the first cycle and (b) after 10 cycles; Figure S14: The boundary potential and state of charge (SOC) performance of different pouch cells; Table S1: The parameters used in the fitting of the high resolution XPS spectra.

Author Contributions: Conceptualization, T.L. and J.Q.; methodology, J.Q.; validation, X.H., Y.Z., T.H. and Y.G.; formal analysis, Y.Z. and T.H.; investigation, T.L. and Y.G.; resources, J.Q.; writing—original draft, T.L.; writing—review and editing, X.H., Y.Z., T.H. and J.Q.; supervision, J.Q.; funding acquisition, T.L. All authors have read and agreed to the published version of the manuscript.

Funding: This research was funded by the Key Research and Development Project of Gansu Natural Energy Research Institute, grant number No. 2021-001, Postdoctoral Research Foundation of Gansu Academy of Sciences (No. BSH2022-02), the Post-doctoral Research Project from Department of Human Resources and Social Security of Gansu Province (No. 302806), and the Open Subject for Key Laboratory of Solar Energy Utilization in Gansu Province in 2024 (No. 2024-006).

Data Availability Statement: The authors confirm that the data supporting the findings of this study are available within the article.

Conflicts of Interest: The authors declare no conflict of interest.

References

1. Hill, C.A.; Such, M.C.; Chen, D.; Gonzalez, J.; Grady, W.M. Battery energy storage for enabling integration of distributed solar power generation. *IEEE Trans. Smart Grid* **2012**, *3*, 850–857. [[CrossRef](#)]
2. Li, X.; Hui, D.; Lai, X. Battery energy storage station (BESS)-based smoothing control of photovoltaic (PV) and wind power generation fluctuations. *IEEE Trans. Sustain. Energy* **2013**, *4*, 464–473. [[CrossRef](#)]

3. Guo, L.; Zhang, Y.; Wang, J.; Ma, L.; Ma, S.; Zhang, Y.; Wang, E.; Bi, Y.; Wang, D.; McKee, W.C.; et al. Unlocking the energy capabilities of micron-sized LiFePO₄. *Nat. Commun.* **2015**, *6*, 7898. [[CrossRef](#)] [[PubMed](#)]
4. Li, J.; Ma, Z.F. Past and present of LiFePO₄: From fundamental research to industrial applications. *Chem.* **2019**, *5*, 3–6. [[CrossRef](#)]
5. Cao, M.; Liu, Z.; Zhang, X.; Yang, L.; Xu, S.; Weng, S.; Zhang, S.; Li, X.; Li, Y.; Liu, T.; et al. Feasibility of prelithiation in LiFePO₄. *Adv. Funct. Mater.* **2023**, *33*, 2210032. [[CrossRef](#)]
6. Xu, K. Nonaqueous liquid electrolytes for lithium-based rechargeable batteries. *Chem. Rev.* **2004**, *104*, 4303–4418. [[CrossRef](#)]
7. Verma, P.; Maire, P.; Novák, P. A review of the features and analyses of the solid electrolyte interphase in Li-ion batteries. *Electrochim. Acta* **2010**, *55*, 6332–6341. [[CrossRef](#)]
8. Yang, Y.; Yan, C.; Huang, J. Research progress of solid electrolyte interphase in lithium batteries. *Acta Phys. Chim. Sin.* **2021**, *37*, 2010076. [[CrossRef](#)]
9. Liu, X.; Tan, Y.; Wang, W.; Li, C.; Seh, Z.W.; Wang, L.; Sun, Y. Conformal prelithiation nanoshell on LiCoO₂ enabling high-energy lithium-ion batteries. *Nano Lett.* **2020**, *20*, 4558–4565. [[CrossRef](#)]
10. Jang, J.; Kang, I.; Choi, J.; Jeong, H.; Yi, K.W.; Hong, J.; Lee, M. Molecularly tailored lithium-arene complex enables chemical prelithiation of high-capacity lithium-ion battery anodes. *Angew. Chem. Int. Ed.* **2020**, *59*, 14473–14480. [[CrossRef](#)]
11. Kim, H.J.; Choi, S.; Lee, S.J.; Seo, M.W.; Lee, J.G.; Deniz, E.; Lee, Y.J.; Kim, E.K.; Choi, J.W. Controlled prelithiation of silicon monoxide for high performance lithium-ion rechargeable full cells. *Nano Lett.* **2016**, *16*, 282–288. [[CrossRef](#)] [[PubMed](#)]
12. Fan, M.; Meng, Q.; Chang, X.; Gu, C.F.; Meng, X.H.; Yin, Y.X.; Li, H.; Wan, L.J.; Guo, Y.G. In situ electrochemical regeneration of degraded LiFePO₄ electrode with functionalized prelithiation separator. *Adv. Energy Mater.* **2022**, *12*, 2103630. [[CrossRef](#)]
13. Zhao, J.; Lu, Z.; Liu, N.; Lee, H.W.; McDowell, M.T.; Cui, Y. Dry-air-stable lithium silicide–lithium oxide core–shell nanoparticles as high-capacity prelithiation reagents. *Nat. Commun.* **2014**, *5*, 5088. [[CrossRef](#)] [[PubMed](#)]
14. Du, J.; Wang, W.; Sheng Eng, A.Y.; Liu, X.; Wan, M.; Seh, Z.W.; Sun, Y. Metal/LiF/Li₂O nanocomposite for battery cathode prelithiation: Trade-off between capacity and stability. *Nano Lett.* **2019**, *20*, 546–552. [[CrossRef](#)]
15. Kulkarni, P.; Jung, H.; Ghosh, D.; Jalalah, M.; Alsaiari, M.; Harraz, F.A.; Balakrishna, R.G. A comprehensive review of prelithiation/sodiation additives for Li-ion and Na-ion batteries. *J. Energy Chem.* **2023**, *76*, 479–494. [[CrossRef](#)]
16. Ding, R.; Tian, S.; Zhang, K.; Cao, J.; Zheng, Y.; Tian, W.; Wang, X.; Wen, L.; Wang, L.; Liang, G. Recent advances in cathode prelithiation additives and their use in lithium-ion batteries. *J. Electroanal. Chem.* **2021**, *893*, 115325. [[CrossRef](#)]
17. Pan, Y.; Qi, X.; Du, H.; Ji, Y.; Yang, D.; Zhu, Z.; Yang, Y.; Qie, L.; Huang, Y. Li₂Se as a cathode prelithiation additive for lithium-ion batteries. *ACS Appl. Mater. Interfaces* **2023**, *15*, 18763–18770. [[CrossRef](#)]
18. Lee, H.; Chang, S.K.; Goh, E.Y.; Jeong, J.Y.; Lee, J.H.; Kim, H.J.; Cho, J.J.; Hong, S.T. Li₂NiO₂ as a novel cathode additive for overdischarge protection of Li-ion batteries. *Chem. Mater.* **2008**, *20*, 5–7. [[CrossRef](#)]
19. Park, K.S.; Im, D.; Benayad, A.; Dylla, A.; Stevenson, K.J.; Goodenough, J.B. LiFeO₂-incorporated Li₂MoO₃ as a cathode additive for lithium-ion battery safety. *Chem. Mater.* **2012**, *24*, 2673–2683. [[CrossRef](#)]
20. Vitins, G.; Raekelboom, E.A.; Weller, M.T.; Owen, J.R. Li₂CuO₂ as an additive for capacity enhancement of lithium ion cells. *J. Power Sources* **2003**, *119*, 938–942. [[CrossRef](#)]
21. Shanmukaraj, D.; Gruegeon, S.; Laruelle, S.; Douglade, G.; Tarascon, J.M.; Armand, M. Sacrificial salts: Compensating the initial charge irreversibility in lithium batteries. *Electrochim. Commun.* **2010**, *12*, 1344–1347. [[CrossRef](#)]
22. Su, K.; Wang, Y.; Yang, B.; Zhang, X.; Wu, W.; Lang, J.; Yan, X. A review: Pre-lithiation strategies based on cathode sacrificial lithium salts for lithium-ion capacitors. *Energy Environ. Mater.* **2023**, *6*, e12506. [[CrossRef](#)]
23. Sun, Y.; Lee, H.W.; Seh, Z.W.; Liu, N.; Sun, J.; Li, Y.; Cui, Y. High-capacity battery cathode prelithiation to offset initial lithium loss. *Nature Energy* **2016**, *1*, 15008. [[CrossRef](#)]
24. Qiao, Y.; Yang, H.; Chang, Z.; Deng, H.; Li, X.; Zhou, H. A high-energy-density and long-life initial-anode-free lithium battery enabled by a Li₂O sacrificial agent. *Nat. Energy* **2021**, *6*, 653–662. [[CrossRef](#)]
25. Bie, Y.; Yang, J.; Wang, J.; Zhou, J.; Nuli, Y. Li₂O₂ as a cathode additive for the initial anode irreversibility compensation in lithium-ion batteries. *Chem. Commun.* **2017**, *53*, 8324–8327. [[CrossRef](#)]
26. Sun, Y.; Lee, H.W.; Seh, Z.W.; Zheng, G.; Sun, J.; Li, Y.; Cui, Y. Lithium sulfide/metal nanocomposite as a high-capacity cathode prelithiation material. *Adv. Energy Mater.* **2016**, *6*, 1600154. [[CrossRef](#)]
27. Ding, R.; Zheng, Y.; Liang, G. Li₂S as a cathode additive to compensate for the irreversible capacity loss of lithium iron phosphate batteries. *Ionics* **2022**, *28*, 1573–1581. [[CrossRef](#)]
28. Park, K.; Yu, B.C.; Goodenough, J.B. Li₃N as a cathode additive for high-energy-density lithium-ion batteries. *Adv. Energy Mater.* **2016**, *6*, 1502534. [[CrossRef](#)]
29. Wang, X.; Liu, C.; Zhang, S.; Wang, H.; Wang, R.; Li, Y.; Sun, J. Dual-functional cathodic prelithiation reagent of Li₃P in lithium-ion battery for compensating initial capacity loss and enhancing safety. *ACS Appl. Energy Mater.* **2021**, *4*, 5246–5254. [[CrossRef](#)]
30. Li, X.; Banis, M.; Lushington, A.; Yang, X.; Sun, Q.; Zhao, Y.; Liu, C.; Li, Q.; Wang, B.; Xiao, W.; et al. A high-energy sulfur cathode in carbonate electrolyte by eliminating polysulfides via solid-phase lithium-sulfur transformation. *Nat. Commun.* **2018**, *9*, 4509. [[CrossRef](#)]

31. Zhan, Y.; Yu, H.; Ben, L.; Chen, Y.; Huang, X. Using Li₂S to compensate for the loss of active lithium in Li-ion batteries. *Electrochim. Acta* **2017**, *255*, 212–219. [[CrossRef](#)]
32. Abouimrane, A.; Dambournet, D.; Chapman, K.W.; Chupas, P.J.; Weng, W.; Amine, K. A new class of lithium and sodium rechargeable batteries based on selenium and selenium–sulfur as a positive electrode. *J. Am. Chem. Soc.* **2012**, *134*, 4505–4508. [[CrossRef](#)] [[PubMed](#)]
33. Wu, F.; Lee, J.T.; Xiao, Y.; Yushin, G. Nanostructured Li₂Se cathodes for high performance lithium-selenium batteries. *Nano Energy* **2016**, *27*, 238–246. [[CrossRef](#)]
34. Park, H.; Kim, J.; Lee, D.; Park, J.; Jo, S.; Kim, J.; Song, T.; Paik, U. Epitaxial growth of nanostructured Li₂Se on lithium metal for all solid-state batteries. *Adv. Sci.* **2021**, *8*, 2004204. [[CrossRef](#)] [[PubMed](#)]
35. Miao, Y.; Sui, Y.; Zhang, D.; Qi, J.; Wei, F.; Meng, Q.; He, Y.; Sun, Z.; Ren, Y. Polyhedral NiCoSe₂ synthesized via selenization of metal-organic framework for supercapacitors. *Mater. Lett.* **2019**, *242*, 42–46. [[CrossRef](#)]
36. Chen, D.; Yue, X.; Li, X.; Wu, X.; Zhou, Y. Research progress of cathode materials for lithium-selenium batteries. *Acta Phys. Chim. Sin.* **2019**, *35*, 667–683. [[CrossRef](#)]

Disclaimer/Publisher’s Note: The statements, opinions and data contained in all publications are solely those of the individual author(s) and contributor(s) and not of MDPI and/or the editor(s). MDPI and/or the editor(s) disclaim responsibility for any injury to people or property resulting from any ideas, methods, instructions or products referred to in the content.